Research Square

Preprints are preliminary reports that have not undergone peer review.
They should not be considered conclusive, used to inform clinical practice,
or referenced by the media as validated information.

Experimental study on damage evolution and post-peak seepage characteristics of gas-bearing coal under horizontal stress compression

Chenxi Liu
Chongqing 208 Geological Environment Research Institute Co., Ltd
Dongming Zhang
zhangdm@cqu.edu.cn
Chongqing University
Mingjun Hu
Chongqing 208 Geological Environment Research Institute Co., Ltd
Beichen Yu
China University of Mining and Technology
Chongyang Wang
Henan Polytechnic University
Wenzhuo Li
Chongqing University
Deqiang Zeng
Chongqing 208 Geological Environment Research Institute Co., Ltd
Zhaoyang Gong
Chongqing University

Article

Keywords: Horizontal compression, True triaxial stress, Permeability, Raw coal, Damage evolution

Posted Date: November 9th, 2026

DOI: https://doi.org/10.21203/rs.3.rs-11343972/v1

License: This work is licensed under a Creative Commons Attribution 4.0 International License.
Read Full License

Additional Declarations: No competing interests reported.

Experimental study on damage evolution and post-peak seepage characteristics of gas-bearing coal under horizontal stress compression

Chenxi Liu[1,2,3], Dongming Zhang [2,3,*], Mingjun Hu[1], Beichen Yu[2,3,4], Chongyang Wang[2,3,5], Wenzhuo Li[2,3],Deqiang Zeng[1], Zhaoyang Gong[2,3]

[1] Chongqing 208 Geological Environment Research Institute Co., Ltd., Chongqing 400700, China.

[2] State Key Laboratory of Coal Mine Disaster Dynamics and Control, Chongqing University, Chongqing 400030, China.

[3] School of Resources and Safety Engineering, Chongqing University, Chongqing 400030, China.

[4] Key Laboratory of Gas and Fire Control for Coal Mines, China University of Mining and Technology, Xuzhou 221116, China

[5] School of Energy Science and Engineering, Henan Polytechnic University, Jiaozuo 454000, China.

*Corresponding author: Dongming Zhang (zhangdm@cqu.edu.cn).

Abstract

Following sedimentation, underground coal seams experience tectonic activity that compresses them horizontally, generating fractures that serve as pathways for coalbed methane migration. Understanding coal seam permeability under horizontal stress compression—especially post-peak permeability—is therefore critical. This study used true triaxial experiments to simulate the deformation and permeability evolution of coal seams under horizontal stress. The loading protocol increased horizontal stress before the peak and gradually decreased it afterward, revealing fracture development during loading and unloading. During loading, pores and fractures compress, increasing particle contact and friction, which promotes fracture initiation and propagation; horizontal compression also reduces primary fracture tortuosity, causing permeability (k) to increase with volumetric strain. During unloading,

as stress is relieved, volumetric deformation decreases, slightly restoring particle and fracture positions, increasing the tortuosity of primary and secondary fractures, and slightly reducing permeability. Based on these characteristics, a damaged coal seam permeability model was proposed. Established using gas pressure and coal seam strain and incorporating a damage factor *D* for both pre- and post-peak segments, the model effectively reveals permeability evolution with changes in strain and gas pressure and fits the experimental results well..

Keywords: Horizontal compression; True triaxial stress; Permeability; Raw coal; Damage evolution.

1. Introduction

Coal is one of the primary sources of energy globally. Taking China as an example, data from the National Bureau of Statistics of China show that coal consumption will account for 55.3% of total energy consumption in 2023, underscoring the importance of coal mines. Therefore, continuous coal production will be necessary in the foreseeable future, along with the further strengthening of coal mine safety[1,2].

Due to geological deposition, underground coal formations undergo various stages of tectonic deformation that determine the developmental characteristics of internal fractures. A common type of compression is horizontal compression, in which coal formations experience sustained stress compression in the horizontal direction, inducing damage and causing the development of numerous internal fractures (Figure 1) [3,4]. The gas within the coal matrix desorbs and diffuses into these fracture channels, promoting gas flow and increasing permeability[5-8]. Therefore, studying the mechanisms by which horizontal stress compression affects the deformation and permeation characteristics of damaged coal bodies is crucial for enhancing coalbed methane extraction efficiency and ensuring efficient and safe mining operations.

Numerous scholars, both domestically and internationally, have extensively researched the permeation characteristics of damaged coal formations[9-11]. Li et al. (2021) investigated the relationship between gas permeation characteristics and coal damage under true triaxial stress and found that, under constant volumetric stress, coal permeability exhibits a parabolic decrease with increasing pore pressure. Bai et al.[13] proposed a new coal permeability model based on the generalized Hooke's law and the Gibbs equation, which comprehensively considered the effects of stress and gas adsorption/desorption. Yu et al.[14] pointed out that although effective stress and permeability are crucial in studying gas-solid coupling in porous media, existing research struggles to accurately reflect the actual stress conditions in geological formations. They studied the effects of induced damage on the effective stress coefficient and permeability of sandstone under true triaxial stress, and confirmed a close relationship between damage evolution and crack propagation. Yang and Huang[15] conducted conventional triaxial permeation tests under different confining pressures and systematically studied intact specimens and those with varying degrees of damage. They found that with increasing axial strain, the permeability of intact sandstone specimens first decreased, then increased, and eventually stabilized. The degree of damage influenced the permeability evolution but did not affect the failure mode of the fractured sandstone, and the permeability increased with gas pressure in the damaged specimens. Yang et al.[16] proposed a stress-damage-flow coupling model that combines changes in stress, damage, and permeability with coal and rock deformation. This model was used to study the deformation and fracture characteristics, permeability, and evolution of airflow in the coal seam cover layers. Wu et al.[17] modified the generalized Hooke's law to consider gas adsorption and thermal expansion effects, establishing a coal damage constitutive relationship based on plastic deformation. They constructed a segmented permeability model

66 considering damage, which effectively reflected the damage evolution law and gas permeation
67 characteristics of coal bodies under different gas pressure conditions. Wang et al.[18] explored the energy
68 evolution law and permeability of damaged coal bodies during mining using conventional triaxial cyclic
69 loading-unloading permeation tests. The results showed that with the stress yield point as the boundary,
70 permeability and the damage variable followed a power function relationship before the yield and an
71 exponential function relationship after the yield. Xue et al.[19] analyzed the differences in permeability
72 evolution between the pre-peak and post-peak stages of coal-rock formations. They established a post-
73 peak permeability model considering damage effects and demonstrated the rationality of the model
74 through a comparative analysis of experimental data and model results. Ye et al.[20] established a coal
75 matrix pore and crack damage-permeation coupling model considering the effects of effective stress, gas
76 adsorption, thermal expansion, and thermal cracks, revealing the evolution of coal permeability under
77 mining disturbances. Cheng et al.[21] improved the fully coupled permeability model of the effective
78 matrix-fracture strain and geometric equations and found that damage in coal instantly accelerated the
79 permeability increase, whereas damage in the matrix slowed it. They concluded that the damage ratio
80 increases with the modulus ratio. An et al.[22] proposed a permeability model that considers stress creep
81 and the effective stress coefficient, revealing the permeability laws under different stress conditions and
82 the influence of creep.

83 Most current research has focused on conventional triaxial experiments under increasing axial stress
84 or stress cycle loading–unloading conditions, revealing the influence of excavation disturbances on the
85 damage characteristics and permeability changes of coal-rock formations. However, under tectonic stress
86 effects, coal-rock formations experience sustained horizontal stress compression, which significantly

affects their stress-strain relationships and permeation characteristics. In actual geological formations, under true triaxial stress conditions, the intermediate principal stress σ_2 greatly affects the horizontal stress state and the deformation and gas flow conditions of coal-rock formations. Therefore, in this study, horizontal stress loading permeation experiments were conducted under true triaxial stress conditions to analyze stress-induced coal body damage deformation and permeability and to establish corresponding permeability models under such conditions.

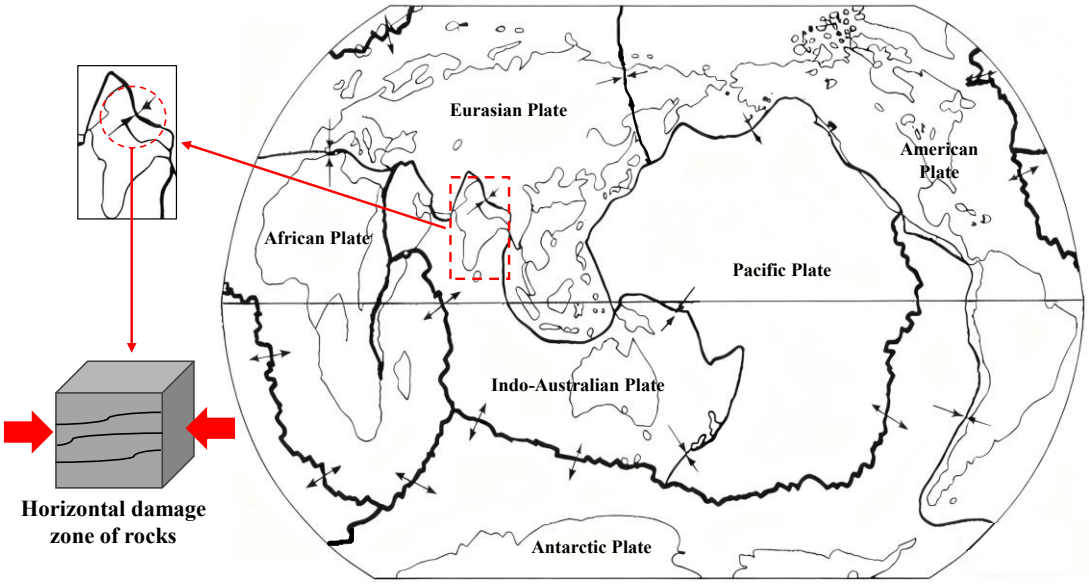


Figure 1. Schematic diagram of coal body damage.

2. Materials and experimental procedures

2.1 Specimen preparation

The coal and rock samples used in the experiments were obtained from a high-quality anthracite coal mine in Sichuan, China, buried at a depth of 490 m. Large original coal samples were cut, cored, and polished to produce standard cubic specimens with dimensions of 100 × 100 × 100 mm. To avoid the influence of end friction effects on the experiment, the unevenness of the cross section was controlled within 0.02 mm, and the specimen surface was smooth without obvious joints or cracks. Prior to the

experiment, strict quality, size, and longitudinal wave velocity tests were performed on the samples. Nine samples were selected with a density difference of less than 0.02 g/cm^2 and a longitudinal wave velocity difference of less than 50 m/s to avoid the influence of rock heterogeneity on the experimental results (Figure 2).

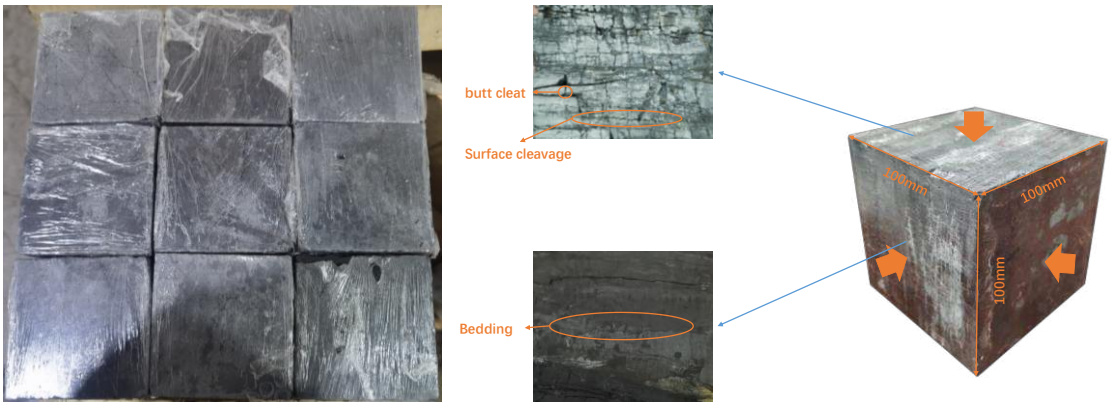


Figure 2. Preparation of specimens.

2.2 Experimental apparatus

A coal-rock permeation experiment was conducted using a multifunctional true triaxial flow-solid coupling test system independently developed by Chongqing University. This system features six loading mechanisms in three directions, each of which can be independently servo-controlled for the loading force, displacement, or mixed loading. It provided a maximum load of 6000 kN in two directions and 4000 kN in one direction, with a fluid pressure capacity of up to 60 MPa. This allows the simulation of various complex stress paths (uniaxial, biaxial, and true triaxial stress states), facilitating the study of coal-rock mechanics, fluid permeation laws, hydraulic fracturing, and other related research. The test system is depicted in Figure 3. In this study, a mixed loading method (force-displacement) was employed to reduce end friction effects[23].

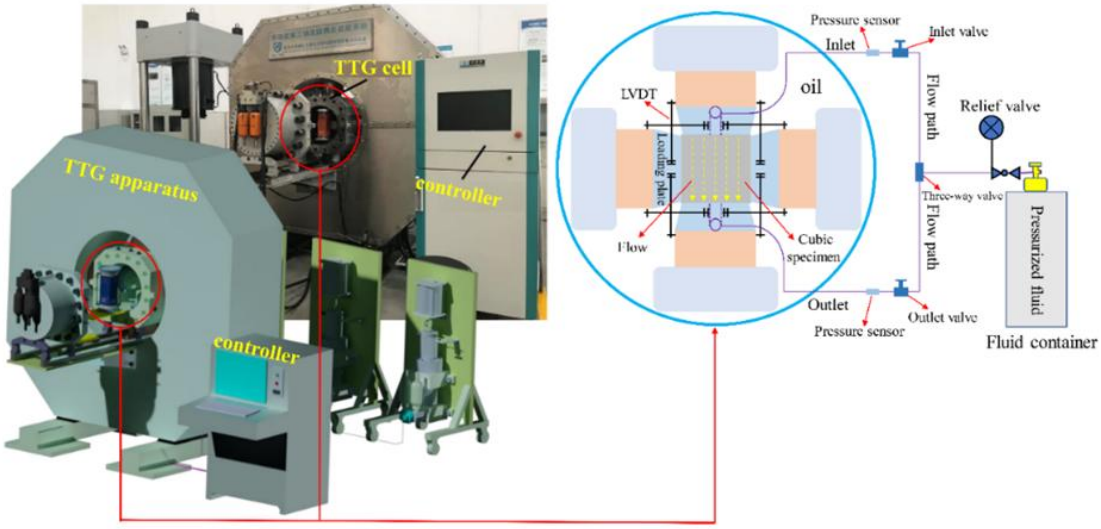


Figure 3. Multifunctional true triaxial fluid-solid coupling test system.

2.3 Experimental procedure

To simulate the damage characteristics and permeability evolution of raw coal under horizontal compression accurately, we established loading methods for both the pre-peak horizontal-stress increase and post-peak gradual horizontal-stress decrease stages. The processed standard specimens were wrapped with heat-shrink tubing to ensure complete isolation from the surrounding environment, and then placed in the loading chamber to begin the experiment. The experimental procedure was as follows.

1) To reduce test variability, each specimen was first subjected to five loading–unloading cycles along the initial maximum horizontal principal stress. This low-stress cyclic loading compacted pre-existing cracks to some extent, thereby minimizing their influence on subsequent permeability measurements.

2) After cyclic loading, to restore the in-situ stress state of the coal sample, three-directional stresses were applied at a loading rate of 0.5 kN/s to simulate the in-situ conditions. The initial stress state was set to σ_Y = 12 MPa, σ_Z = 10 MPa, and σ_X = 8 MPa.

3) While maintaining the stress conditions of the coal sample, gas pressures of P = 1, 2, and 3 MPa were applied axially to simulate the presence of gas in the coal seam.

4) Loading was applied in the direction of the intermediate principal stress at a rate of 0.5 kN/s until the stress curve exhibited significant non-linear characteristics, indicating that the coal body entered the plastic stage.

5) Horizontal stress unloading along the direction of the intermediate principal stress was performed at 0.5 kN/s until the stress curve returned to the initial rock stress state. The damage evolution and permeability variation processes of the rock mass before and after the peak were analyzed.

Using this method, three groups of true triaxial permeability tests were conducted, and the median value of the results of the three coal samples in each group was obtained. The test parameters for each group are listed in Table 1. The stress loading path and experimental diagram are shown in Figure 4. During the test, the direction of stress loading was parallel to the bedding plane, and the direction of penetration was perpendicular to the bedding plane.

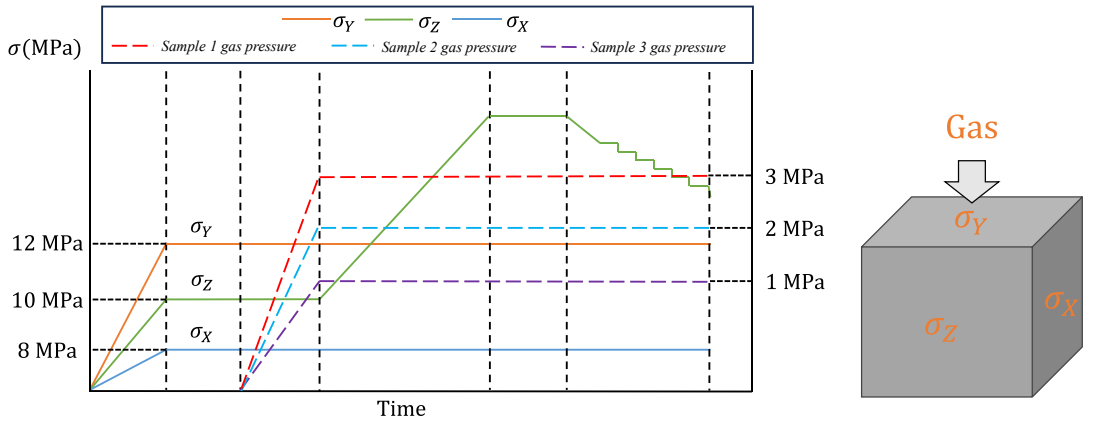
Helium was used as the injection gas to eliminate the effects of gas adsorption. The exit flow rate was recorded using a mass flowmeter, and Darcy's law was applied to calculate the permeability of the coal body under different true triaxial stress conditions. The formula is as follows:

$$k = \frac{2Q\mu LP_2}{A(P_1^2 - P_2^2)} \tag{1}$$

where k is the permeability of the coal body (m^2), Q is the gas flow rate under standard conditions (m^3/s), μ is the dynamic viscosity of the gas (Pa·s), L is the length of the coal sample specimen (m), A is the cross-sectional area of the coal sample specimen (m^2), P_1 is the pressure at the helium gas inlet (Pa), and P_2 is the atmospheric pressure (Pa).

Table 1. Experimental testing parameters

Test	P(MPa)	Stress condition
1	1	σ_Y = 12 MPa , σ_Z = 10 MPa , σ_X = 8 MPa
2	2	σ_Y = 12 MPa , σ_Z = 10 MPa , σ_X = 8 MPa
3	3	σ_Y = 12 MPa , σ_Z = 10 MPa , σ_X = 8 MPa



(a) (b)

Figure 4. Stress and gas pressure loading and unloading path diagram: (a) Stress loading and unloading path; (b) Stress loading and unloading orientation diagram.

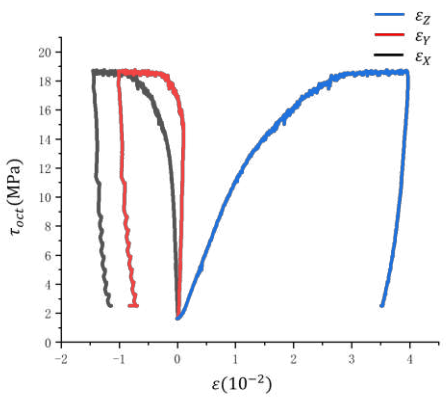
3. Experimental results and analysis

3.1 Analysis of stress-strain characteristics of coal under horizontal stress loading

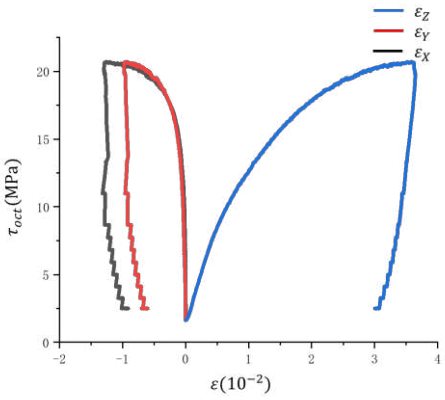
The stress–strain responses of the coal specimens under true triaxial horizontal stress loading–unloading tests are shown in Figure 5. The vertical axis τ_{oct} denotes the octahedral shear stress, defined as $\frac{1}{3}\sqrt{(\sigma_x-\sigma_y)^2+(\sigma_x-\sigma_z)^2+(\sigma_y-\sigma_z)^2}$, where σ_x, σ_y, σ_z are the stresses in the X, Y and Z directions, respectively. ε_x, ε_y, ε_z, represent the corresponding strains in the X, Y and Z directions. Figures 5(a), 5(b) and 5(c) present the stress-strain curves at gas pressures of 1, 2 and 3 MPa, respectively.

In Figure 5, the negative abscissa represents expansion under specific stress conditions, while the positive abscissa represents compression. Under the action of external applied stress, the z-direction was continuously compressed, whereas the other two directions exhibited expansion. When the z-direction

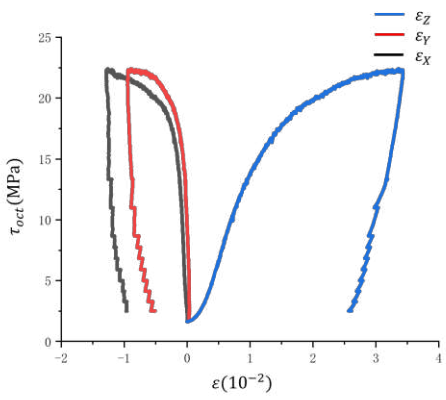
stress was gradually unloaded, the compressive strain in the z-direction decreased, and the expansion deformation in the other two directions also diminished; however, the strain in each direction did not return to the origin. This indicates that as the z-direction stress increased, the resistance of the coal to the applied stress enhanced, leading to the initiation and propagation of internal cracks and thus causing varying degrees of internal damage. With the reduction in z-direction stress, the residual elastic deformation within the coal, as well as the positions of particles and cracks, underwent slight recovery, resulting in decreased compressive deformation in the z-direction and reduced expansion deformation in the other two directions. Nevertheless, due to the internal damage induced by the loading process, the deformation resistance of the coal was weakened, leading to the failure of strains in all directions to return to the origin.

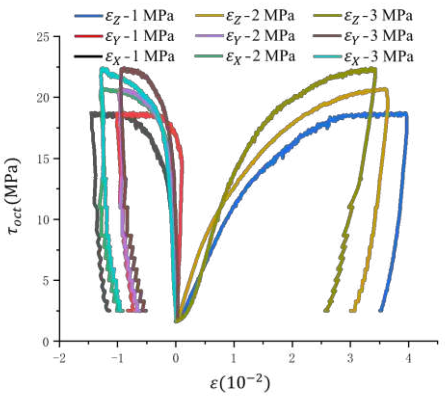


(a)



(b)





(c) (d)

Figure 5. Stress-strain curve of coal under horizontal stress loading: (a) Gas pressure P = 1 MPa; (b) Gas pressure P = 2 MPa; (c) Gas pressure P = 3 MPa; (d) Gas pressures of P = 1 MPa, 2 MPa, and 3 MPa.

As the gas pressure increased, the stress was counteracted and the coal body expanded. To analyze the effect of gas pressure on coal deformation, axial gas pressures of 1, 2, and 3 MPa were applied to the coal samples during the experiment, and the deformation of each group was observed. First, it was essential to calculate the volume strain of the coal body under each gas pressure condition. The volume strain offers a comprehensive reflection of the overall deformation of the coal body, providing a deeper understanding of deformation patterns under specific conditions and laying the foundation for analyzing the expansion effect. The formula for calculating the volume strain is as follows:

$$\varepsilon_V = \varepsilon_Y + \varepsilon_X + \varepsilon_Z \tag{2}$$

where ε_Y, ε_Z, and ε_X represent the strain in the Y-, Z-, and X-directions, respectively.

The volumetric strain (ε_V) of the rock samples in each experimental group was calculated using Equation (2) and is illustrated in Figure 6(a). The curves demonstrate that during the pre-peak stage, an increase in gas pressure (P) results in a decrease in the overall volumetric strain (ε_V) of the coal body. This indicates that, in the pre-peak stage, the counteractive effect of the gas pressure on the stress becomes more pronounced, leading to an expansion effect that causes the coal body to expand, thereby reducing its volumetric strain.In the post-peak stage, the (ε_V) of the three coal body groups gradually increases. This is attributed to the coal bodies resisting stress, which leads to internal damage. Because stress was applied in the Z-direction, the extent of damage in the Z-direction was greater than that in the other directions. During unloading in the Z-direction, the diminished ability to resist deformation due to

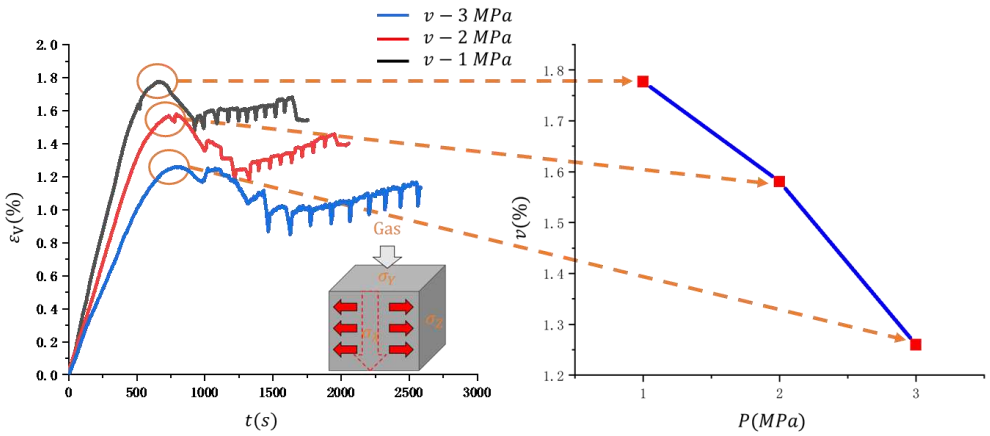
damage results in a relatively smaller decrease in deformation resistance in the other two directions, causing a rebound in the (ε_V) values.

To further elucidate the effects of gas expansion, the compression ratios of the coal bodies in each group under different gas pressures were calculated using the following formula:

$$v = \frac{\Delta V}{V} \tag{3}$$

where v represents the compression ratio of the coal body, V represents the initial volume of the coal body (m^3), and ΔV represents the change in volume of the coal body after compression (m^3).

Using Equation (3), the changes in coal compressibility before and after the peak were calculated to observe the influence of the expansion effect on the volume strain under different gas pressures. The calculation results are presented in Figure 6(b).



(a) (b)

Figure 6. Volume compression ratio strain curves under different gas pressures: (a) Overall compression ratio; (b) Compression ratio peak value.

As the gas pressure increased, the stress response and deformation capacity of coal became more pronounced. At a gas pressure of 3 MPa, the peak compression ratio of coal was approximately 1.3%; at 2 MPa, the peak compression ratio ranged between 1.7% and 1.8%; and at 1 MPa, it ranged between 1.8%

and 1.9%. These changing curves indicate that as the gas pressure increased, the coal compression ratio gradually decreased, enhancing its expansion effect and thereby increasing its resistance to deformation, leading to higher peak stresses.

Throughout the loading-unloading process, the curves did not return to their original baseline, further indicating that the coal underwent irreversible plastic deformation and permanent damage. Analysis of the stress-strain curve characteristics revealed that under axial gas pressure, the coal's resistance to deformation increased with increasing gas pressure. Owing to the influence of the horizontal Z-directional stress loading, the degree of damage in the Z-direction was higher, resulting in a more significant reduction in the deformation resistance.

During stress loading and gradual unloading, coal damage and changes in permeability must be considered via the strain, permeability, and damage effects during the unloading stages. This aids in a deeper understanding of the deformation behavior and permeability changes in gas-containing coal under horizontal stress compression and holds significant research importance for coal mine safety and enhancing coalbed methane extraction efficiency.

3.2 Analysis of coal permeability characteristics

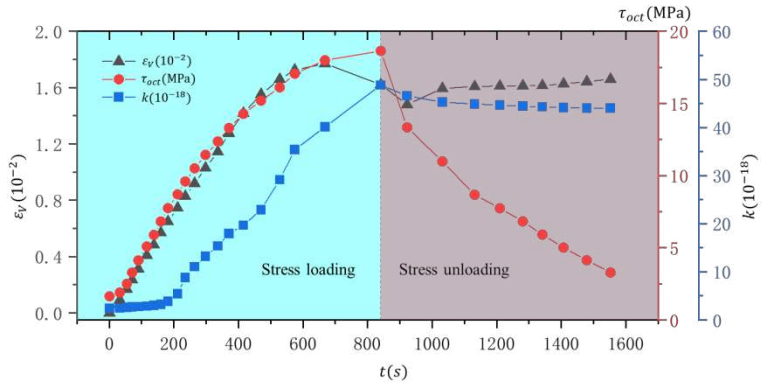
To accurately study the process of rock mass movement and variations in coal permeability, it is necessary to analyze changes in coal permeability under the combined effects of horizontal stress loading–unloading and different gas pressures[24-26]. This approach primarily aims to characterize changes in coal permeability by analyzing deformation. Curves of coal volumetric strain, octahedral shear stress, permeability, and their variations with loading time are shown in Figure 7.

It can be seen from Figure 7 that permeability exhibited a gradual increasing trend prior to the peak

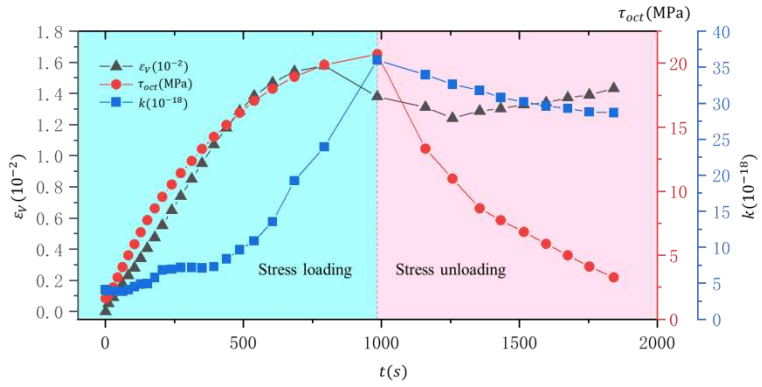
stress. The closer the octahedral shear stress was to the peak stress, the more pronounced the change in permeability. Furthermore, during the period when octahedral shear stress increased before reaching the peak stress, volumetric strain decreased while permeability increased significantly. This phenomenon occurred because the coal specimens were loaded primarily in the Z-direction. When the coal specimens entered the yield stage, increasing stress induced the development of internal fractures, resulting in damage to the coal matrix. Consequently, the expansion deformation in the X and Y directions exceeded the compressive deformation in the Z-direction.

After the peak stress, permeability showed a gradual decreasing trend. This is attributed to the gradual unloading of stress, which promoted the recovery of elastic deformation within the coal and an increase in the tortuosity of internal fissures. The combined effect of these two factors led to a gradual decrease in permeability. At this stage, volumetric strain first decreased and then gradually increased. This trend arose because when unloading initially began and the coal was not yet fully damaged, elastic potential energy was stored within the coal. This caused the expansion deformation in the Z-direction to be greater than the compressive deformation in the X and Y directions, resulting in a decrease in volumetric strain.

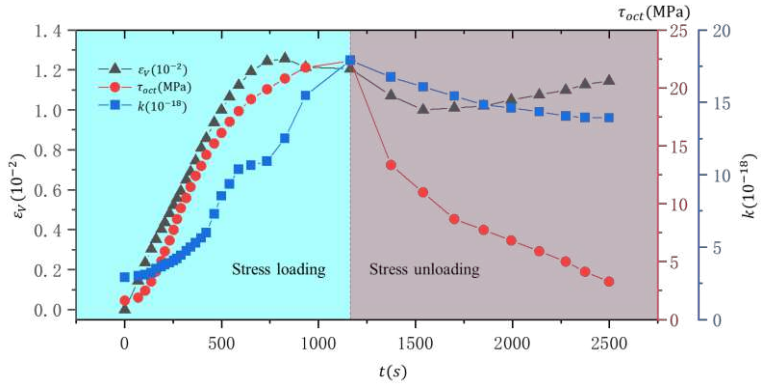
As stress was gradually unloaded, the release of elastic potential energy diminished. In the later stage of unloading, deformation was mainly determined by changes in strain in the X, Y, and Z directions. Since the Z-direction was the primary loading direction, it sustained more severe damage. Therefore, the expansion deformation in the Z-direction was smaller than the compressive deformation in the X and Y directions, leading to an increase in volumetric strain.



(a)



(b)



(c)

Figure 7. Curves of coal volume strain and permeability variation: (a) Gas pressure P = 1 MPa; (b) Gas pressure P = 2 MPa; (c) Gas pressure P = 3 MPa.

To better understand the meaning represented by the trend of the permeability curve in Figure 7. An explanation for this trend is depicted in Figure 8, with red arrows indicating the gas flow pathways. In the initial coal state, the spacing between coal particles was stable, allowing the gas to pass smoothly

through the channels to the outlet. In the original rock stress state, compression causes the redistribution of coal particles, narrowing of gas channels, and reduced permeability. In the initial compression state of the intermediate principal stress, the gas flow direction was perpendicular to the horizontal stress direction. As compression proceeded, the tortuosity of the pore fractures decreased, resulting in increased gas permeability. In the intermediate principal stress compressive damage state induced by the intermediate principal stress, the contact area between particles increases, and the friction between particles increases, promoting the initiation and expansion of fractures, which enhances the gas channels and increases permeability. During the intermediate principal stress step-by-step unloading stage, a slight recovery of the particle and fracture positions occurs, increasing the tortuosity of both the primary and secondary fractures, thus slightly reducing the permeability. Because the experiment involved gas flowing into the coal during the original rock stress stage, the observed trend in permeability was consistent with these changes.

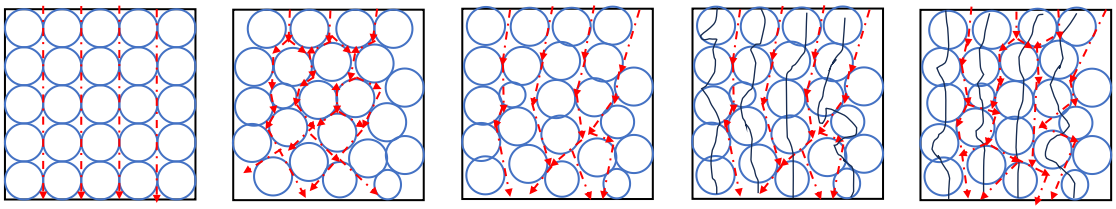


Figure 8. Gas channel state in coal body at different stress stages: (a) Initial state of coal; (b) Original rock stress state; (c) Initial compression state of intermediate principal stress; (d) Intermediate principal stress compressive damage state; (e) Intermediate principal stress step by step unloading stage.

In this study, the Z-direction was designated as the primary loading–unloading stress direction. It was more strongly affected by the applied stress than the other two directions and therefore exerted a

more pronounced influence on permeability evolution. To better examine the relationship between stress, strain, and permeability in this direction during the loading–unloading process, the curves of horizontal stress, strain, and permeability in the Z-direction are illustrated in Figure 9. As the Z-directional stress gradually increased, the permeability first increased slowly and then rose rapidly, exhibiting an approximately exponential growth trend, while the strain in this direction displayed a relatively smooth increasing tendency. During the subsequent unloading stage, the damage induced in the coal led to only minor changes in Z-directional strain and permeability, and the relationships among stress, strain, and permeability showed a trend of rapid decrease followed by gradual decrease.

The evolution of permeability under different gas pressures is also presented in Figure 9. When the gas pressure was 1 MPa, both the peak permeability and its variation amplitude were the largest, whereas at 3 MPa, both the peak permeability and its variation amplitude were the smallest. This indicates that with increasing gas pressure, the ability of the gas to counteract stress-induced deformation was enhanced, causing permeability to decrease with increasing gas pressure and thus providing a certain protective effect on the coal. In addition, when the gas pressure was 3 MPa, the post-peak reduction in permeability was not pronounced, mainly because the high gas pressure offset the increase in fracture tortuosity induced by stress unloading.

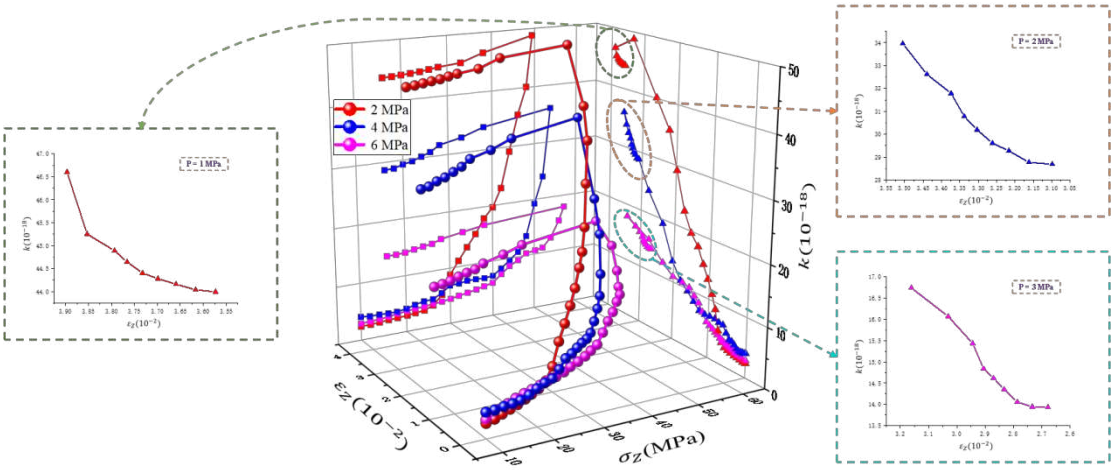


Figure 9. The relationship between horizontal stress-strain and permeability

Overall, as the horizontal stress increased, the horizontal strain in the Z-direction, and the volumetric strain both increased, leading to an increase in permeability before the peak. The formation of fractures during the initial loading stage contributed to the enhancement of permeability. The increase in fracture tortuosity caused by horizontal stress unloading resulted in a slight reduction in permeability. With increasing gas pressure, permeability gradually decreased, indicating that higher gas pressure suppressed the reduction in volumetric strain induced by horizontal stress, thereby reducing the number of gas flow pathways and ultimately lowering permeability.

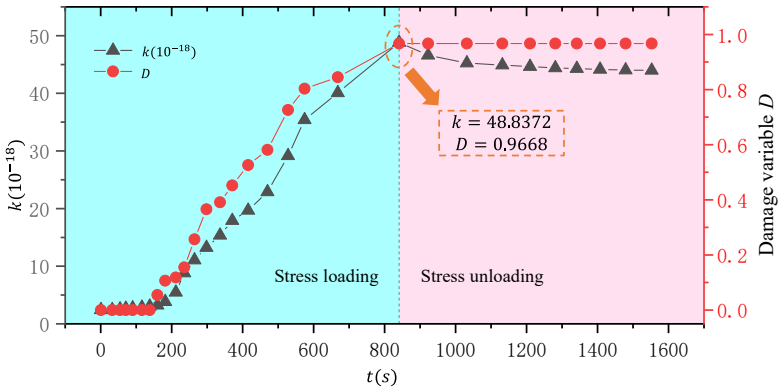
4. Discussion

4.1 Process of Damage Evolution

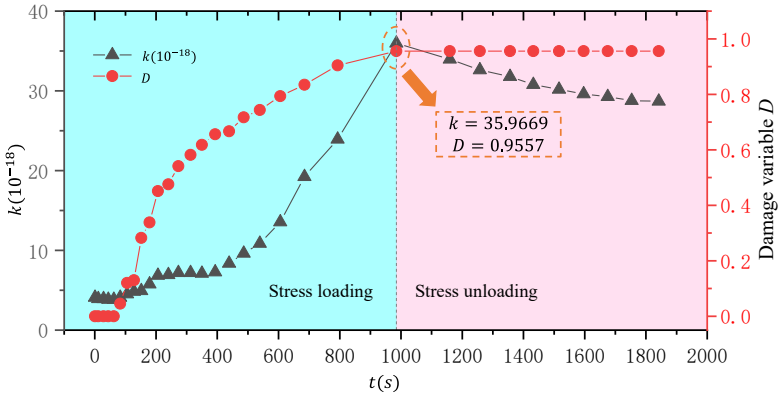
Through the study of the stress-strain characteristics and permeability characteristics of coal during the horizontal stress loading–unloading process, it can be seen that the force exerted on the coal during the experiment caused a certain degree of irreversible damage. To clearly observe the changes in coal body damage during the test process, the damage variables in the simplified model of the equivalent elastic damage flexibility tensor defined by Hu et al.[27] and applied by Wang and Kong et al.[28,29] will be referred to below. The calculation formula for the damage variable is as follows:

$$D = 1 - \frac{\tilde{E}}{E_0} \tag{4}$$

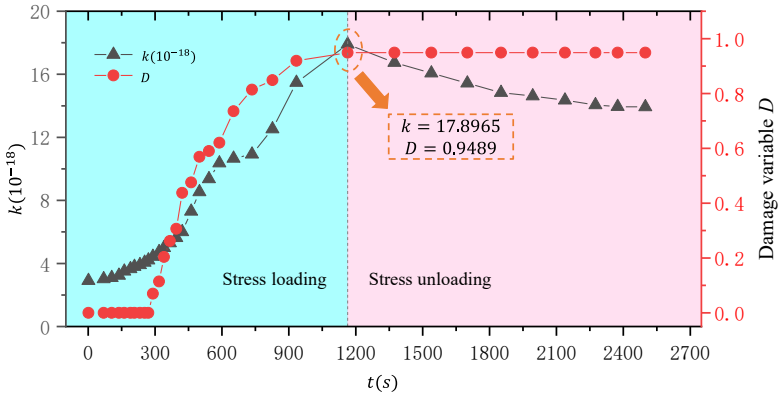
where E_0 is the elastic modulus of the undamaged material (Pa), $\tilde{E}$ is the elastic modulus of the damaged material (Pa), and D is the damage variable.



(a)



(b)



(c)

Figure 10. Change of coal body damage variable D under different air pressure: (a) Gas pressure P = 1 MPa; (b) Gas pressure P = 2 MPa; (c) Gas pressure P = 3 MPa.

The variation trend of the coal damage variable D under different gas pressures was obtained through Equation (4), as shown in Figure 10. It can be seen from Figure 10 that the trend of D under each pressure condition is characterized by an initial constant phase, followed by a rapid increase, and then a gentle rise as it approaches the peak stress. Due to the irreversibility of damage, the damage variable does not decrease but remains unchanged during the horizontal stress unloading of the coal. To study the relationship between permeability and the damage variable, the permeability change rate is the permeability value under the current stress state, and is the permeability value at the peak stress was introduced to analyze the stress unloading stage (Figure 11). The reason for selecting this stage for investigation is that the damage variable values in Figure 10 vary with different gas pressures, yet remain constant during the stress unloading stage itself. Therefore, by comparing the permeability change rate during the stress unloading process, the influence of the damage variable on the permeability characteristics of coal can be reflected and analyzed.

The variation trend of the coal damage variable D under different gas pressures was obtained through calculation Equation (4), as shown in Figure 10. It can be seen from Figure 10 that the trend under each pressure condition is characterized by an initial constant phase, followed by a rapid increase, and then a gentle rise as it approaches the peak. Due to the irreversibility of damage, the damage factor does not decrease but remains unchanged during the horizontal stress unloading process of the coal body. To study the relationship between permeability and the damage variable, the permeability change rate Δk ($\triangle k = \frac{k_{max}-k_i}{k_{max}}$, where k_i is the permeability value under the current stress state, k_{max} is the permeability value at the peak stress) was introduced to analyze the stress unloading stage (Figure 11).

The reason for selecting this stage for investigation is that the damage variable in Figure 10 differs under different gas pressures, while its value does not change during the stress unloading stage itself. Therefore, by comparing the change rate of permeability during the stress unloading process, the influence of the damage factor on the permeability characteristics of coal can be reflected and analyzed.

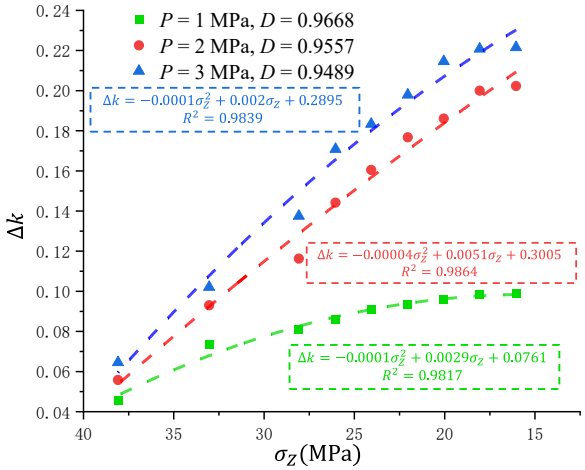


Figure 11. Rate of Permeability Change during Unloading

Figure 10 shows that when the gas pressure P is 1, 2, and 3 MPa, the damage variable D of the coal is 0.9668, 0.9557, and 0.9489, respectively. From Figure 11, it can be observed that when the gas pressure P is 3 MPa and the damage variable D is 0.9489, the increase in the permeability change rate Δk during stress unloading is more significant than that under other gas pressures. This indicates that under this condition, the coal sustains the least damage and exhibits stronger recoverability. When the horizontal stress of the coal is unloaded to its lowest point, the permeability change rate Δk is 0.09914, 0.20233, and 0.22154, corresponding to damage variables D of 0.9668, 0.9557, and 0.9489, respectively. These results indicate that a larger damage variable corresponds to a smaller permeability change rate and lower restorability of the coal.

4.2 Establishment of a permeability model for damaged coal bodies

Studying the evolution of permeability in damaged coal rock before and after its peak value is crucial for ensuring mine safety and enhancing gas extraction efficiency. By understanding the variations in permeability associated with coal rock damage and establishing accurate permeability models, it is possible to effectively predict and control gas diffusion and migration, thereby avoiding gas-related hazards[30-34]. To investigate the evolution of permeability in the damaged coal rock before and after its peak, we primarily utilized the classical permeability model proposed by Shi and Durucan[35]. This model employs the average normal stress and gas pressure to represent permeability as follows:

$$\frac{k}{k_0} = \exp[-3C_f(\sigma_{em} - \sigma_{em0})] \tag{5}$$

where C_f is the fracture compressibility constant (MPa^{-1}), σ_m is the effective stress (MPa), σ_{m0} is the initial effective stress (MPa), p is the gas pressure (Pa).

The relationship between the average normal stress and the total stress is as follows:

$$\sigma_{em} = \sigma_m - \beta p \tag{6}$$

where σ_m is the total stress (MPa), β is the effective stress coefficient, p is the gas pressure (Pa).

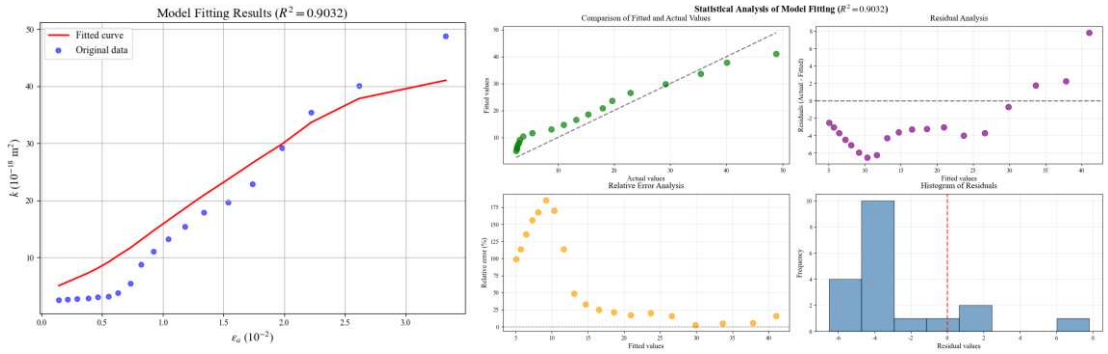
According to the previous analysis, coal is damaged by stress during the loading process. The damage variable D can reflect changes in permeability. Therefore, the damage variable D is introduced here. Based on damage mechanics theory and the one-dimensional linear elastic damage model of materials[36,37], combined with Equation (4), the following formula is derived:

$$\varepsilon_m = \frac{\sigma_m}{\tilde{E}} \tag{7}$$

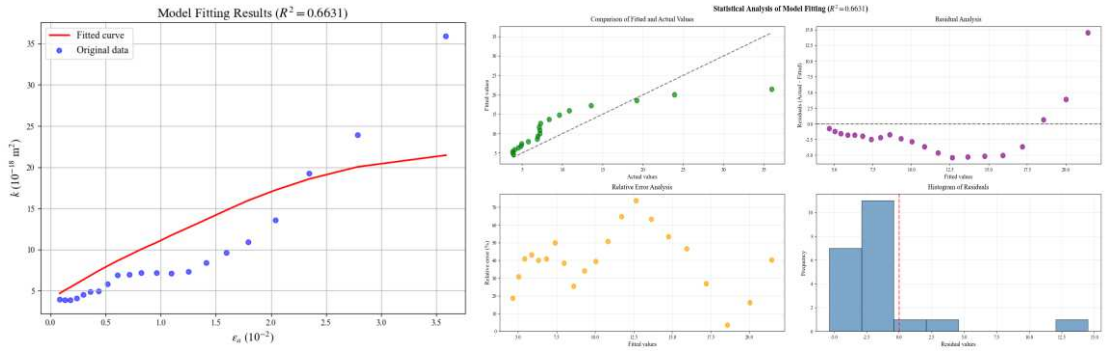
By combining Equations (4), (5), (6), and (7), we obtain

$$k = k_0 \cdot \exp\{-3C_f[(\varepsilon_m E_0(1-D) - \beta p) - (\sigma_{m0} - \beta p)]\} \tag{8}$$

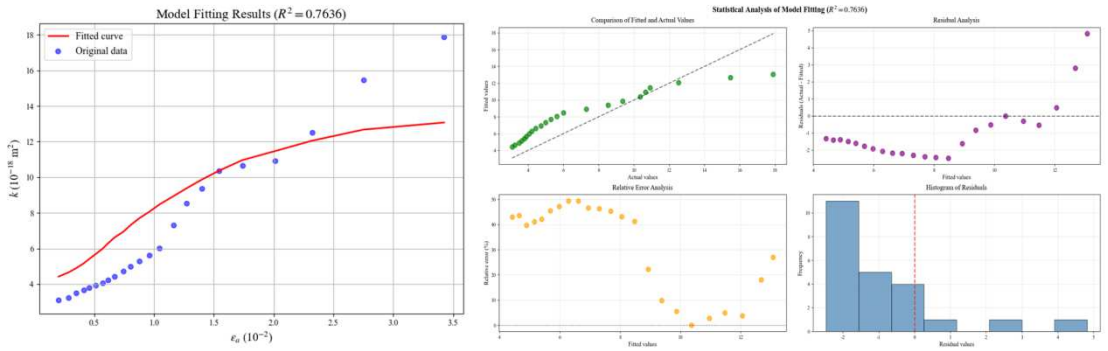
The main research object of this study is the influence of horizontal stress on the permeability characteristics of coal. Therefore, the stress and strain values in the horizontal Z-direction were substituted into the model for calculation, and the results obtained are shown in Figure 12.



(a)



(b)



(c)

Figure 12. Fitting curve of the permeability model: (a) Gas pressure P = 1 MPa; (b) Gas pressure P = 2 MPa; (c) Gas pressure P = 3 MPa.

The fitting results presented in Figure 12 indicate suboptimal model performance. Under the three different gas pressures, the highest R^2 value for permeability fitting was only 0.9032, while the other two R^2 values were merely 0.6631 and 0.7636. To improve the model's accuracy, an optimization factor was incorporated into the permeability formula. Candidate functions for this factor—including a constant term, a linear function, a Tanh function, and a Sigmoid function—were individually introduced into the permeability model for fitting and comparison. The comparative analysis showed that integrating the Sigmoid function achieved the best improvement in the model's fitting performance. The formula for this optimization factor is as follows:

$$C(\varepsilon_m) = C_0 + \frac{C_1 - C_0}{1 + e^{-h\cdot(\varepsilon_m - i)}} \tag{9}$$

where C_0, C_1, h, and i are all fitting parameters that need to be fitted in the subsequent calculation, and by combining Equations (8) and (9), we obtain

$$k = k_0 \cdot \exp\{-3C(\varepsilon_m)C_f\,[(\varepsilon_m E_0\,(1 - D) - \beta p) - (\sigma_{m0} - \beta p)]\} \tag{10}$$

Next, the permeability model for the stress unloading stage (i.e., the post-peak stress stage) is established. The evolution of post-peak permeability in coal is influenced by various factors, including coal failure modes, loading control modes, fracturing degree, and fracture connectivity. Currently, few theoretical models based on classical mechanics can adequately characterize the evolution of post-peak permeability in coal [38]. Yin et al.[39] tested the gas permeation velocity in coal during the full stress-strain process under different in situ stress conditions and established a quadratic polynomial fitting relationship between post-peak gas permeation velocity and axial stress.

$$Q_a = l\sigma_m^2 + m\sigma_m + n \tag{11}$$

where Q_m is the gas flow rate under standard conditions (mL/s), and l, m, and n are fitting coefficients.

Based on Darcy's law, the post-peak coal permeability is related to gas permeation as follows:

$$k = \frac{2Q_a \mu L P_a}{A(p_0^2 - p^2)} \tag{12}$$

where μ is the dynamic viscosity of the gas (Pa·s), L is the length of the coal sample specimen (m), A is the cross-sectional area of the coal sample specimen (m^2), p is the gas pressure (Pa), p_0 is the initial gas pressure (Pa), and P_a is the atmospheric pressure (Pa).

Equation (12) is derived as follows. Assuming that the gas flow in the core is steady and the process is isothermal, the mass flow rate of the gas through each cross section remains constant. According to the Boyle–Mariotte law, we obtain

$$QP = Q_a P_a = \text{constant} \ \text{ or } \ Q = Q_a P_a / P \tag{13}$$

where Q_a is the volumetric gas flow rate at the atmospheric pressure P_a. Substituting Equation (13) into Darcy's law, we obtain

$$k = -\frac{Q_a P_a \mu}{PA} \frac{dL}{dP} \tag{14}$$

By separating the variables in Equation (14) and integrating, we obtain:

$$\int_{p_0}^{p} KP dP = -\int_0^L \frac{Q_a P_a \mu}{A} dL \tag{15}$$

After integration and simplification, we obtain Equation (12). By combining Equations (11) and (12), we obtain

$$k = \frac{2(l\sigma_m^2 + m\sigma_m + n)\mu L P_a}{A(p_0^2 - p^2)} \tag{16}$$

During the pre-peak stress loading process, the coal body undergoes damage, which also affects the post-peak permeability. Therefore, the formula for the post-peak permeability calculation must introduce

the damage factor D by combining Equations (4) and (16).

$$k = \frac{2[l(\varepsilon_a \tilde{E})^2 + m(\varepsilon_a \tilde{E}) + n]\mu L P_a}{A(p_0^2 - p^2)} \tag{17}$$

Considering the permeability characteristics of the coal body before and after the peak stage, based on Equations (10) and (17), the theoretical model for the full stress-strain permeability of the damaged coal body can be derived:

$$k = \begin{cases} k = k_0 \cdot \exp\{-3C(\varepsilon_m)C_f\,[(\varepsilon_m E_0\,(1-D) - \beta p) - (\sigma_{m0} - \beta p)]\,\}(\varepsilon_a \le \varepsilon_p) \\ \dfrac{2[l(\varepsilon_a \tilde{E})^2 + m(\varepsilon_a \tilde{E}) + n]\mu L P_a}{A(p_0^2 - p^2)}(\varepsilon_a > \varepsilon_p) \end{cases} \tag{18}$$

where ε_p represents the onset of post-peak strain softening. Many fitting parameters are present in Equation (18). For example, parameters l, m, and n are fitting parameters determined from the permeability results using a quadratic polynomial relationship. These parameters are closely related to the damage characteristics, porosity, and fracture connectivity of coal. The permeability calculation model is divided into two stages: pre- and post-peak. The upper equation in Equation (18) is mainly used for calculations in the pre-peak stage, whereas the lower equation is mainly used for calculations in the post-peak stage.

4.3 Validation of the damaged coal permeability model results

To better fit the parameters in the damage evolution and permeability models, the Levenberg–Marquardt (LM) algorithm is employed. The LM algorithm is a method for solving non-linear least squares problems, particularly those that are ill-conditioned[40-44]. It is commonly used for curve fitting because it improves the Gauss–Newton method to handle optimization problems more effectively.

The Gauss–Newton method aims to minimize the sum of squares of residuals in a least squares problem, where a set of observed values y is compared to model predictions $f(x,\alpha)$. Here, x represents the

known independent variable, and α denotes the model parameters to be fitted. The objective is to find the parameters α that minimize the sum of squared residuals[45-49].

$$S(\alpha) = \sum_i [y_i - f(x_i, \alpha)]^2 \quad (19)$$

This method iteratively searches for parameters that minimize the sum of the squared residuals. In each iteration, a linear approximation of the residuals is constructed, and the parameters are updated to minimize the sum of the squares of the approximate residuals. Each update step is expressed as

$$\Delta\alpha = (J^T J)^{-1} J^T r \quad (20)$$

where J is the Jacobian matrix, whose elements J_{ij} are partial derivatives of f with respect to the parameter α_j, and r is the residual vector.

The LM method introduces a damping factor, λ, which merges the Gauss–Newton method with gradient descent. This damping factor is adjusted during iterations; it decreases when nearing the minimum, aligns more closely with the Gauss–Newton method, and increases further from the minimum, ensuring a better descent direction. The parameter transformation is expressed as

$$\Delta\alpha = [J^T J + \lambda diag(J^T J)]^{-1} J^T r \quad (21)$$

where diag($J^T J$) represents a diagonal matrix composed of the diagonal elements of matrix $J^T J$.

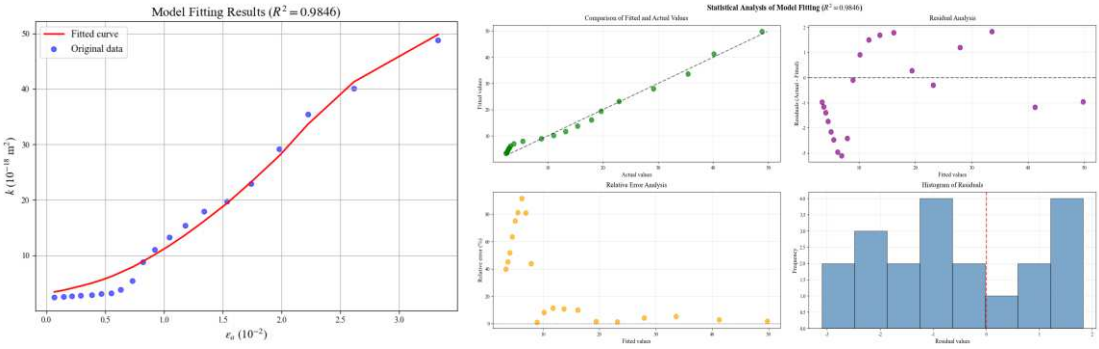
By adjusting λ, the algorithm can enhance the stability of the search direction in situations where the Gauss–Newton method may be unstable. By incorporating historical data into Equation (18) and applying the LM algorithm for fitting, the fitting results of historical data are shown in Figure 13(a)–(c), which represent the relationship between the strain and permeability change under gas pressures P = 1, 2, and 3 MPa, respectively, before the peak. Figure 14(a)–(c) show the relationship between the strain

and permeability changes under gas pressures P = 1, 2, and 3 MPa, respectively, after the peak. In Figures 13 and 14, the blue dots represent the experimental data and the red line represents the fitting curve. The fitting curves can be examined to determine whether they generally meet the prediction requirements. The basic parameters for each coal sample are listed in Table 2.The relationship between the damage variable D and the permeability and strain of the coal at pressure P = 1, 2, and 3 MPa is shown in Figures 10(a) - (c).

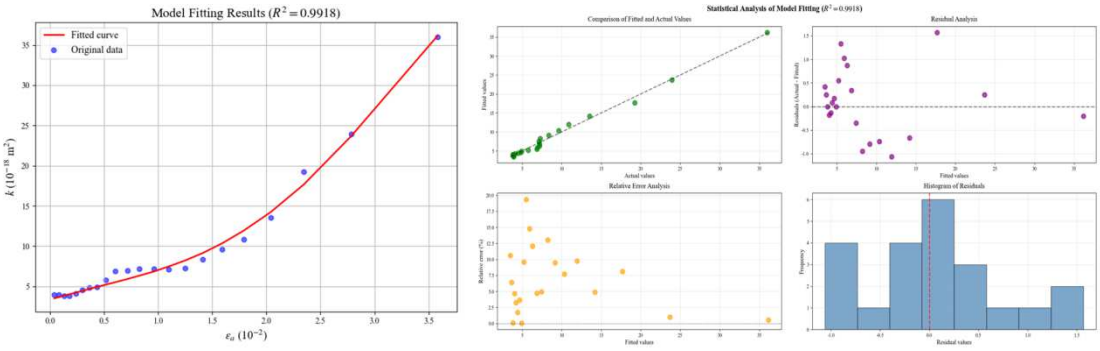
Table 2. Basic parameters of coal

Group	Elastic modulus E/GPa	the fracture compressibility constant C_f/MPa^{-1}
Group 1	4.7449	-0.01970
Group 2	4.9469	-0.01278
Group 3	4.8168	-0.00835

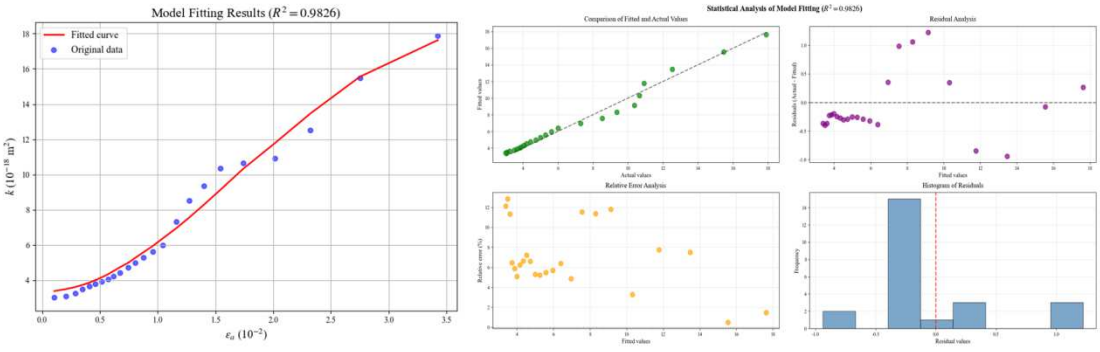
The fitting parameters for the stress loading stage are shown in Table 3, with no abnormal values observed among the parameters. As can be seen from Figure 13, the permeability model exhibits a good fitting effect during the stress loading stage. The goodness of fit R^2 reaches 0.9846, 0.9918, and 0.9826 at gas pressures of 1, 2, and 3 MPa, respectively. The goodness of fit of this model is significantly higher than that of the permeability model without the optimization factor, and the numerical variation range of the residual analysis is also relatively narrower. This indicates that the model can better reflect the permeability changes caused by coal damage during the stress loading stage.



(a)



(b)



(c)

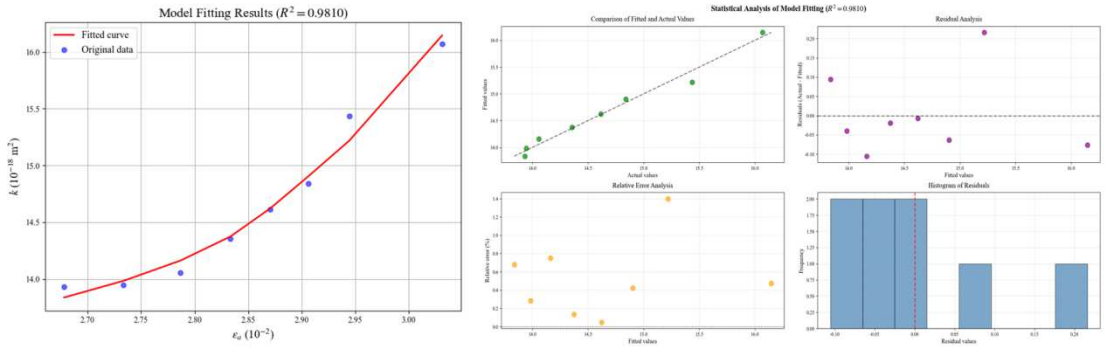
Figure 13. Goodness-of-fit test curve of coal permeability in the stress loading stage: (a) Gas pressure P = 1 MPa; (b) Gas pressure P = 2 MPa; (c) Gas pressure P = 3 MPa.

Table 3. Coal pre-peak fitting parameters

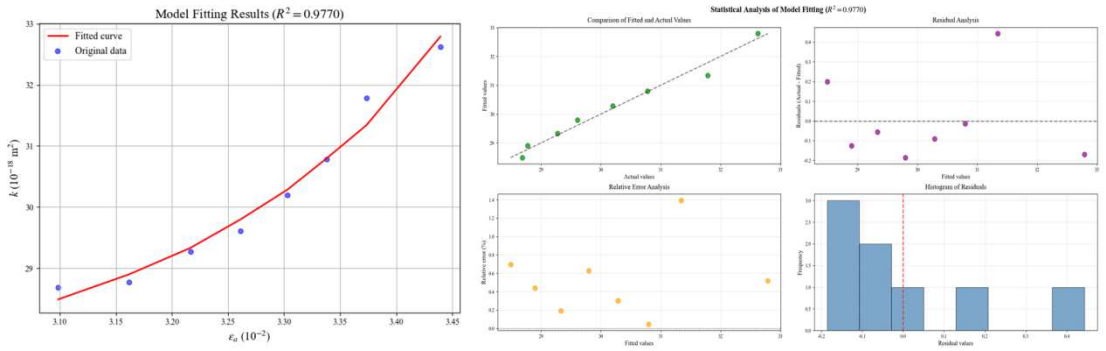
Group	Fitting parameters C_0	Fitting parameters C_1	Fitting parameters h	Fitting parameters i	The gas pressure coefficient β

Group 1	0.1022	1.1032	0.9999	0.0681	0.5103
Group 2	0.4619	1.4801	1.0000	2.3331	0.5764
Group 3	-0.7206	1.2787	1.0000	0.1050	0.6182

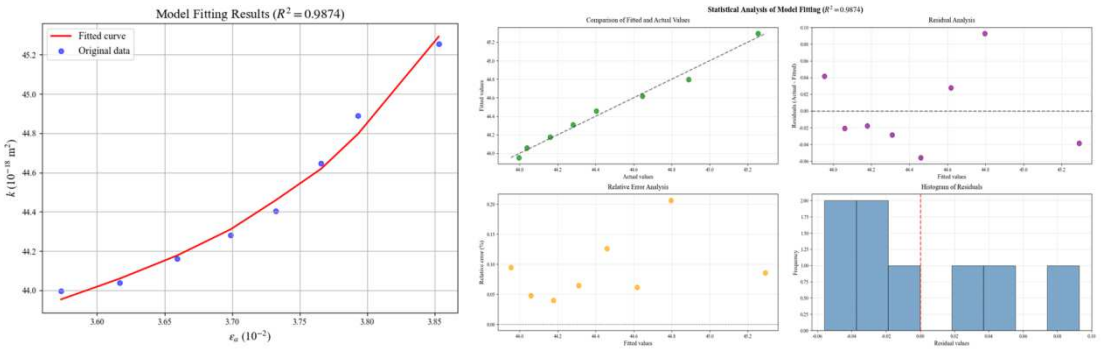
The fitting parameters for the stress unloading stage are shown in Table 4, with no abnormal values observed among the parameters. As can be seen from Figure 14, the permeability model exhibits a good fitting effect during the stress unloading stage. The goodness of fit R^2 reaches 0.9810, 0.9770, and 0.9874 at gas pressures of 1, 2, and 3 MPa, respectively. The numerical variation range of the residual analysis is also relatively narrower. This indicates that the model can also accurately reflect the permeability changes caused by coal damage during the stress unloading stage.



(a)



(b)



(c)

Figure 14. Goodness-of-fit test curve of coal body permeability in the stress unloading stage: (a) Gas pressure P = 1 MPa; (b) Gas pressure P = 2 MPa; (c) Gas pressure P = 3 MPa.

Table 4. Post-peak fitting parameters of coal

Group	Fitting parameters l	Fitting parameters m	Fitting parameters n
Group 1	1.06×10^{-4}	-4.56×10^{-4}	2.6247
Group 2	1.93×10^{-4}	5.73×10^{-3}	1.5729
Group 3	2.35×10^{-4}	-4.34×10^{-3}	0.8367

From the fitting results of the permeability model for coal during the stress loading and unloading stages in this study, it can be seen that the goodness of fit R^2 exceeds 0.97 in both stages. This indicates that the proposed model has high prediction accuracy for coal permeability before and after the peak stress, meeting the needs of permeability prediction and providing support for the study of coal permeability characteristics under horizontal stress loading–unloading.

5. Conclusion

This research is divided into two distinct stages: the stress loading stage (i.e., the pre-peak stage), which simulates the continuous horizontal stress compression experienced by underground coal seams during various stages of sedimentation and tectonic activities, resulting in the development of numerous fractures and an increase in permeability; the stress unloading stage (i.e., the post-peak stage), which

505 simulates the permeability recovery driven by the horizontal stress unloading induced by mining
506 activities. The main conclusions drawn from the experimental results are as follows:

507 (1) Analysis of the stress-strain curves of coal under different gas pressures reveals that the stress
508 required for coal to reach the yield stage increases with increasing gas pressure. In addition, gas pressure
509 induces an expansion effect in coal, resulting in a decrease in the compression ratio with increasing gas
510 pressure. Although strain decreased during the stress unloading stage, the stress-strain curve did not
511 return to the original baseline due to irreversible plastic deformation and permanent damage to coal.

512 (2) During the pre-peak phase, the horizontal stress loading induced plastic deformation in the coal
513 seam. Initially, this process compressed the internal pores and fractures, increasing the contact area and
514 friction between the particles, which facilitates the initiation and propagation of cracks. Concurrently,
515 the stress loading reduced the tortuosity of the internal pores and fractures within the coal seam.
516 Consequently, the gas flow channels expanded, resulting in an increase in permeability (k) as the
517 volumetric strain increased. In the post-peak phase, as the stress was gradually unloaded, the volumetric
518 deformation decreased, and the unloading of the horizontal stress caused a minor recovery in the positions
519 of the particles and fractures. This resulted in an increased curvature and slightly reduced permeability
520 in both primary and secondary fractures.

521 (3) A damage permeability evolution model was established based on strain and gas pressure, and
522 the permeability analysis was divided into two stages: stress loading stage and unloading stage. This
523 model incorporates damage factors to establish a permeability framework and utilizes fitting algorithms
524 to determine model parameters. Goodness-of-fit tests for the fitted curves yielded pre-peak correlation
525 coefficients R^2 of 0.9846, 0.9918, and 0.9826, and post-peak correlation coefficients R^2 of 0.9810, 0.9770,

and 0.9874, which all exceed 0.97. These results validate that the established formulas accurately reflect the changes in permeability.

Declarations

Funding. This study was financially supported by the Scientific Research Foundation of State Key Laboratory of Coal Mine Disaster Dynamics and Control (2011DA105287-zd201804) and the National Science and Technology Major Project of Deep Earth from the Department of Science and Technology Development, Ministry of Natural Resources of the People's Republic of China (2025ZD1011303).

Competing interests. We declare we have no competing interests.

Ethics statement. It is not relevant to my work.

Data Availability Statement. The experimental data supporting the conclusions are available from the corresponding author on request.

Acknowledgments

Acknowledgement for the data support from " China Earthquake Disaster Prevention Center, Seismic Active Fault Survey Data Center. (https://www.activefault-datacenter.cn)".

Credit Author Statement

Conceptualization: [Chenxi Liu], [Beichen Yu];

Methodology: [Chenxi Liu], [Wenzhuo Li];

Formal analysis and investigation: [Beichen Yu], [Chongyang Wang];

Writing - original draft preparation: [Chenxi Liu], [Wenzhuo Li];

Writing - review and editing: [Chenxi Liu], [Mingjun Hu];

Funding acquisition: [Dongming Zhang], [Mingjun Hu];

Resources: [Dongming Zhang];

Supervision: [Zhaoyang Gong], [Deqiang Zeng].

References

1. Li, B., Chai, Z., Gao, M., & Lyu, Q. Technological Empowerment Revitalizes Fossil Energy with 'Green' Vitality. *Frontiers of Science*, *16*(2), 30-34. https://doi.org/10.3969/j.issn.1673-8128.2022.02.008 (2022).
2. Suo, Y., Li, S., Jin, C., Zhang, Y., Zhou, J., Li, X., Wang, P., Liu, Z., Wang, X., & Somerville, I. Eastward tectonic migration and transition of the Jurassic-Cretaceous Andean-type continental margin along Southeast China. *Earth-Science Reviews*, *196*, 102884. https://doi.org/10.1016/j.earscirev.2019.102884 (2019).
3. Huang, Q., Wu, B., Cheng, W., Lei, B., Shi, H., & Chen, L. Investigation of permeability evolution in the lower slice during thick seam slicing mining and gas drainage: a case study from the Dahuangshan coalmine in China. *Journal of Natural Gas Science and Engineering*, *52*, 141-154. https://doi.org/10.1016/j.jngse.2018.01.036 (2018).
4. Yuan, L. Strategic Reflections on Deep Coal and Gas Co-Production in China. *Journal of Coal Science*, *41*(1), 1-6. https://doi.org/10.13225/j.cnki.jccs.2015.9027 (2016).
5. Jiang, F., Yin, Y., Zhu, Q., Wang, C., & Qu, X. Experimental Study on Coal and Gas Outburst Early Warning Based on Dynamic Changes of Face Stress and Gas Concentration. *Rock Mechanics and Engineering, 33*(s2), 3581-3588. https://doi.org/10.13722/j.cnki.jrme.2014.s2.023 (2014).
6. Ma, N., Zhao, X., Zhao, Z., Guo, X., Liu, H., & Jia, H. Hypothesis on the Mechanism of Butterfly-type Coal and Gas Outbursts in Drivage Roadways. *Journal of Mining Science*, *2*(2), 137-149. https://doi.org/10.13545/j.cnki.jmse.2017.02.009 (2017).
7. Xue, Y., Gao, F., Liu, X., & Liang, X. Permeability and pressure distribution characteristics of the roadway surrounding rock in the damaged zone of an excavation. *International Journal of Mining Science and Technology*, *27*(2), 211-219. https://doi.org/10.1016/j.ijmst.2017.01.003 (2017).
8. Zhang, H., Cheng, Y., Liu, Q., Yuan, L., Dong, J., Wang, L., Qi, Y., & Wang, W. A novel in-seam borehole hydraulic flushing gas extraction technology in the heading face: Enhanced permeability mechanism, gas flow characteristics, and application. *Journal of Natural Gas Science and Engineering*, *46*, 498-514. https://doi.org/10.1016/j.jngse.2017.08.022 (2017).
9. Agostinetti, N. P., Bianchi, I., Amato, A., & Chiarabba, C. Fluid migration in continental subduction: The Northern Apennines case study. *Earth and Planetary Science Letters*, *302*(3-4), 267-278. https://doi.org/10.1016/j.epsl.2010.10.039 (2011).
10. Luo, C. H., Wang, R., Zhao, Y., Huang, J., & Evans, N. J. Mobilization of Cu in the continental lower crust: A perspective from Cu isotopes. *Geoscience Frontiers*, *14*(5), 101590. https://doi.org/10.1016/j.gsf.2023.101590 (2023).
11. Shu, L., Wang, K., Qi, Q., & Zhang, L. Evolution Characteristics of Stress Field on Coal Drivage Face and Evaluation Model of Outburst Hazard. *Journal of Mining & Safety Engineering*, *34*(2),

259-267. https://doi.org/10.13545/j.cnki.jmse.2017.02.009 (2017).
12. Li, X, Nie, B., Liu, F., Wang, G., Tian, J., & Niu, P. The relation of gas seepage and coal body damage under the true three dimension stress. *Procedia Engineering*, *26*, 1462-1466. https://doi.org/10.1016/j.proeng.2011.11.2324 (2011).
13. Bai, X., Wang, Y., He, G., Zhou, Z., Wang, D., & Zhang, D. Research on a permeability model of coal damaged under triaxial loading and unloading. *Fuel*, *354*, 129375. https://doi.org/10.1016/j.fuel.2023.129375 (2023).
14. Yu, B., Zhang, D., Xu, B., Li, M., Liu, C., & Xiao, W. Experimental study on the effective stress law and permeability of damaged sandstone under true triaxial stress. *International Journal of Rock Mechanics and Mining Sciences*, *157*, 105169. https://doi.org/10.1016/j.ijrmms.2022.105169 (2022).
15. Yang, S. Q., & Huang, Y. H. Effect of damage on gas seepage behavior of sandstone specimens. *Journal of Rock Mechanics and Geotechnical Engineering*, *12*(4), 866-876. https://doi.org/10.1016/j.jrmge.2020.02.003 (2020).
16. Yang, T. H., Xu, T., Liu, H. Y., Tang, C. A., Shi, B. M., & Yu, Q. X. Stress–damage–flow coupling model and its application to pressure relief coal bed methane in deep coal seam. *International Journal of Coal Geology*, *86*(4), 357-366. https://doi.org/10.1016/j.coal.2011.04.002 (2011).
17. Wu, X., Li, B., Wang, X., Gao, Z., Li, J., & Xu, J. Research on Coal Damage Constitutive Relationship and Permeability Model Based on Plastic Deformation. *Coal Geology and Exploration*, *49*(6), 131-141. https://doi.org/10.3969/j.issn.1001-1986.2021.06.016 (2021).
18. Wang, X., Zhou, H., Zhong, J., Zhang, L., & An, L. Energy Evolution and Permeability Characteristics of Deep Coal Damage under Triaxial Cycling Loading and Unloading. Journal of *Rock Mechanics and Engineering*, *37*(12), 2676-2684. https://doi.org/10.13722/j.cnki.jrme.2018.0697 (2018).
19. Xue, Y., Gao, F., Gao, Y., & Liang, X. Research on Evolution Model of Post-Peak Permeability of Damaged Coal-Rock Mass under Mining Influence. *Journal of China University of Mining and Technology*, *46*(3), 521-527. https://doi.org/10.13247/j.cnki.jcumt.000681 (2017).
20. Ye, P., Li, B., Ren, C., Song, H., Fu, J., & Wu, X. Investigation on damage-permeability model of dual-porosity coal under thermal-mechanical coupling effect. *Gas Science and Engineering*, *123*, 205229. https://doi.org/10.1016/j.jgsce.2024.205229 (2024).
21. Cheng, X., Luan, H., Chen, L., Zhang, J., & Jiang, Y. Impact of coal damage on permeability evolution based on an improved permeability model. *Journal of Natural Gas Science and Engineering*, *101*, 104509. https://doi.org/10.1016/j.jngse.2022.104509 (2022).
22. An, C., Killough, J., & Xia, X. Investigating the effects of stress creep and effective stress coefficient on stress-dependent permeability measurements of shale rock. *Journal of Petroleum Science and Engineering*, *198*, 108155. https://doi.org/10.1016/j.petrol.2020.108155 (2021).
23. Yu, B., Zhang, D., Zhao, K., Xu, B., Geng, J., Wang, C., & Chen, Y. Experimental study on stress and permeability response with gas depletion in coal seams. *Journal of Natural Gas Science and Engineering*, *108*, 104824. https://doi.org/10.1016/j.jngse.2022.104824 (2022b).
24. Palmer, I. Permeability changes in coal: analytical modeling. *International Journal of Coal Geology*, *77*(1-2), 119-126. https://doi.org/10.1016/j.coal.2008.09.006 (2009).
25. Pan, Z., & Connell, L. D. Modelling permeability for coal reservoirs: a review of analytical models

627 and testing data. *International Journal of Coal Geology*, *92*, 1-44.
628 https://doi.org/10.1016/j.coal.2011.12.009 (2012).
629 26. Wang, G. G., Zhang, X., Wei, X., Fu, X., Jiang, B., & Qin, Y. A review on transport of coal seam gas
630 and its impact on coalbed methane recovery. *Frontiers of Chemical Science and Engineering*, *5*,
631 139-161. https://doi.org/10.1007/s11705-010-0527-4 (2011).
632 27. Hu, S., Wang, E., & Kong, X.Damage and deformation control equation for gas-bearing coal and its
633 numerical calculation method. *Journal of Natural Gas Science and Engineering*, *25*, 166-179.
634 https://doi.org/10.1016/j.jngse.2015.04.039 (2015).
635 28. Kong, X., Wang, E., Liu, Q., Li, Z., Li, D., Cao, Z., & Niu, Y. Dynamic permeability and porosity
636 evolution of coal seam rich in CBM based on the flow-solid coupling theory. *Journal of Natural*
637 *Gas Science and Engineering*, *40*, 61-71. https://doi.org/10.1016/j.jngse.2017.02.011 (2017).
638 29. Wang, E., Kong, X., Hu, S., Li, Z., & Liu, Q. Multi-scale fractured coal gas–solid coupling model
639 and its applications in engineering projects. *Transport in Porous Media*, *121*, 703-724.
640 https://doi.org/10.1007/s11242-017-0981-2 (2018a).
641 30. Chen, D., Pan, Z., Shi, J. Q., Si, G., Ye, Z., & Zhang, J. A novel approach for modelling coal
642 permeability during transition from elastic to post-failure state using a modified logistic growth
643 function. *International Journal of Coal Geology*, *163*, 132-139.
644 https://doi.org/10.1016/j.coal.2016.07.007 (2016).
645 31. Liu, L., Zhu, W., Wei, C., & Ma, X. Mechanical Model and Numerical Analysis of Gas Adsorption-
646 Induced Coal Strength Deterioration. *Rock and Soil Mechanics*, *39*(4), 1500-1508.
647 https://doi.org/10.16285/j.rsm.2017.0335 (2018).
648 32. Zhang, N., Li, X., Cheng, H., & Teng, T. A coupled damage-hydro-mechanical model for gas drainage
649 in low-permeability coalbeds. *Journal of Natural Gas Science and Engineering*, *35*, 1032-1043.
650 https://doi.org/10.1016/j.jngse.2016.09.050 (2016).
651 33. Zhang, X. M., Zhang, D. M., Leo, C. J., Yin, G. Z., Feng, D., & Liyanapathirana, D. S. Damage
652 evolution and post-peak gas permeability of raw coal under loading and unloading conditions.
653 *Transport in Porous Media*, *117*, 465-480. https://doi.org/10.1007/s11242-017-0842-z (2017).
654 34. Zhu, W., Liu, L., Liu, J., Wei, C., & Peng, Y. Impact of gas adsorption-induced coal damage on the
655 evolution of coal permeability. *International Journal of Rock Mechanics and Mining Sciences*, *101*,
656 89-97. https://doi.org/10.1007/s00603-013-0392-9 (2018).
657 35. Shi, J., Durucan, S. Drawdown induced changes in permeability of coalbeds: a new interpretation of
658 the reservoir response to primary recovery[J]. Transport in porous media, 2004, 56(1): 1-16.
659 http://doi.org.10.1023/B:TIPM.0000018398.19928.5a (2004).
660 36. Li, Z., Li, H., & Xiong, Z. Damage constitutive model of mico- and meso-cracks of coal sample.
661 *Nonferrous Metals(Mine Section)*, *55*(5), 15-17 (2003).
662 37. Li, X, Nie, B., Liu, F., Wang, G., Tian, J., & Niu, P. The relation of gas seepage and coal body damage
663 under the true three dimension stress. *Procedia Engineering*, *26*, 1462-1466.
664 https://doi.org/10.1016/j.proeng.2011.11.2324 (2011).
665 38. Zhou, H., Rong, T., Mou, R., Wang, L., & Ren, W. Construction and Research Progress of Coal
666 Permeability Model under Mining Stress. *Journal of China Coal Society*, *44*(1), 221-235.
667 https://doi.org/10.13225/j.cnki.jccs.2018.5029 (2019).
668 39. Yin, G., Huang, Q., Zhang, D., & Wang, D. Experimental Study on Gas Permeation Characteristics

during Deformation and Failure Process of Gas-Bearing Coal-Rock in Geostress Field. *Journal of Rock Mechanics and Engineering*, *29*(02), 336-343. https://doi.org/JournalArticle/5af591eec095d718d826b3a8 (2010).

40. Chen, J., Jiang, Z., & Que, Y. Hierarchical recursive Levenberg–Marquardt algorithm for radial basis function autoregressive models. *Information Sciences*, *647*, 119506. https://doi.org/10.1016/j.ins.2023.119506 (2023).
41. Tian, Y., Xia, J., Sun, Y., Wang, X., Du, Q., Bai, W., Wang, D.,Cai, Y., Wu, C., Li, F., & Qiao, H. Improved specular point prediction precision using gradient descent algorithm. *Advances in Space Research*, *65*(6), 1568-1579. https://doi.org/10.1016/j.asr.2019.12.016 (2020).
42. Verma, S., Thampi, G. T., & Rao, M. ANN based method for improving gold price forecasting accuracy through modified gradient descent methods. *IAES International Journal of Artificial Intelligence*, *9*(1), 46. https://doi.org/10.11591/ijai.v9.i1.pp46-57. (2020).
43. Ye, Z., & Kim, M. K. Predicting electricity consumption in a building using an optimized back-propagation and Levenberg–Marquardt back-propagation neural network: Case study of a shopping mall in China. *Sustainable Cities and Society*, *42*, 176-183. https://doi.org/10.1016/j.scs.2018.05.050 (2018)
44. Žic, M., Vlašić, L., Subotić, V., Pereverzyev, S., Fajfar, I., & Kunaver, M. Extraction of distribution function of relaxation times by using Levenberg-Marquardt algorithm: A new approach to apply a discretization error free Jacobian matrix. *Journal of The Electrochemical Society*, *169*(3), 030508. https://doi.org/10.1149/1945-7111/ac55c9 (2022).
45. Gonçalves, M. L., & Menezes, T. C. Gauss–Newton methods with approximate projections for solving constrained nonlinear least squares problems. *Journal of Complexity*, *58*, 101459. https://doi.org/10.1016/j.jco.2020.101459 (2020).
46. Mittal, G., & Giri, A. K. Convergence rates for iteratively regularized Gauss–Newton method subject to stability constraints. *Journal of Computational and Applied Mathematics*, *400*, 113744. https://doi.org/10.1016/j.cam.2021.113744 (2022).
47. Pes, F., & Rodriguez, G. A doubly relaxed minimal-norm Gauss–Newton method for underdetermined nonlinear least-squares problems. *Applied Numerical Mathematics*, *171*, 233-248. https://doi.org/10.1016/j.apnum.2021.09.002. (2022).
48. Wang, H., & Wang, Q. A new Gauss--Newton-like method for nonlinear equations. *Turkish Journal of Mathematics*, *45*(1), 264-280. https://doi.org/10.3906/mat-1912-68 (2021).
49. Wang, Y. Maximum likelihood computation based on the Fisher scoring and Gauss–Newton quadratic approximations. *Computational statistics & data analysis*, *51*(8), 3776-3787. https://doi.org/10.1016/j.csda.2006.12.037. (2007).

Authors and Affiliations

Chenxi Liu[1,2,3], Dongming Zhang [2,3,*], Mingjun Hu[1], Beichen Yu[2,3,4], Chongyang Wang[2,3,5], Wenzhuo Li[2,3],Deqiang Zeng[1], Zhaoyang Gong[2,3]

[1] Chongqing 208 Geological Environment Research Institute Co., Ltd., Chongqing 400700, China.

[2] State Key Laboratory of Coal Mine Disaster Dynamics and Control, Chongqing University, Chongqing 400030, China.

[3] School of Resources and Safety Engineering, Chongqing University, Chongqing 400030, China.

[4] Key Laboratory of Gas and Fire Control for Coal Mines, China University of Mining and Technology, Xuzhou 221116, China

[5] School of Energy Science and Engineering, Henan Polytechnic University, Jiaozuo 454000, China.

*Corresponding author: Dongming Zhang (zhangdm@cqu.edu.cn).